electronics

MDPI

Article

Model-Free Hybrid Control with Intelligent Proportional Integral and Super-Twisting Sliding Mode Control of PMSM Drives

Peng Gao [1,2], Guangming Zhang [1,*] and Xiaodong Lv [1]

[1] College of Electrical Engineering and Control Science, Nanjing Tech University, Nanjing 211899, China; 201862107015@njtech.edu.cn (P.G.); 201962107002@njtech.edu.cn (X.L.)
[2] College of Electrical Engineering, Tongling University, Tongling 244061, China
* Correspondence: zgm@njtech.edu.cn

Received: 18 July 2020; Accepted: 31 August 2020; Published: 2 September 2020

Abstract: In this research, based on the ultra-local model, a novel compound model-free control strategy with an intelligent Proportional-Integral and super-twisting Sliding Mode Control (MFiPISTSMC) strategy for permanent magnet synchronous motor (PMSM) drives is proposed. Firstly, an intelligent Proportional-Integral (iPI) control strategy is designed for motor speed regulation. Secondly, a super-twisting Sliding Mode Control (STSMC) strategy is constructed based on the ultra-local model of PMSM. At the same time, the unknown term of the ultra-local model of PMSM is estimated by a Linear Extended State Observer (LESO). The stability of the compound MFiPISTSMC strategy is proved by the Lyapunov stability theorem. As a result of the compound MFiPISTSMC strategy integrating the STSMC strategy, the iPI control strategy and the LESO is proposed to have excellent performance. Finally, the static characteristic, dynamic characteristic and robustness of the novel compound MFiPISTSMC strategy are verified by simulation and experimental results.

Keywords: model-free control; super-twisting Sliding Mode Control (STSMC); intelligent Proportional-Integral (iPI); permanent magnet synchronous motor (PMSM); Linear Extended State Observer (LESO)

1. Introduction

Due to some advantages, such as simple structure, small volume, high efficiency, and high power factor, the permanent magnet synchronous motor (PMSM) has been widely used in many applications such as in aerospace actuation [1], electric vehicles [2,3], and suspended positioning systems [4].

Because of the invention of the PMSM, a multitude of scholars have not stopped studying control strategies. Many control theories have been widely and effectively applied to the speed regulation system of the PMSM, which can be roughly divided into two categories: model-related control and model-free control (MFC). More precisely, for the model-related control, a host of scholars used the mathematical model of the PMSM to deeply analyze various advanced controllers; examples of such algorithms include, model predictive control [5], backstepping control [6], nonlinear adaptive control [7], $H\infty$ robust control [8], and so on. However, the external loads and internal parameters are variable in the actual working environment. Consequently, the PMSM cannot be accurately represented by the mathematical model, which bring challenges and troubles to the model-related control. In recent years, the MFC strategy has been more and more popular. Although the MFC strategy was introduced only a few years ago, the traditional Proportional-Integral (PI) control strategy, as the most widely used MFC strategy, has been widely applied in the PMSM speed regulation system [9,10]. However, the traditional PI control strategy may cause the PMSM speed control system to deviate

from the expected target due to the nonlinearity, time variability, and complexity of the PMSM drives. Based on an ultra-local model, an intelligent Proportional-Integral (iPI) control strategy was proposed in reference [11]. The iPI control strategy based on the ultra-local mode has been widely used in the control of various systems: see, e.g., single link flexible joint manipulator [12], quadrotor vehicle [13], and laser beam pointing and stabilization [14]. Unfortunately, the iPI control strategy cannot guarantee that the tracking error of the system tends to zero quickly. To overcome this problem, Reference [15] integrated the advantages of the MFC strategy, the iPI control strategy and the Sliding Mode Control (SMC) strategy, a compound iPI-SMC control strategy based on the MFC theory (MFiPISMC) was proposed, which effectively solves the problem that the iPI control strategy cannot quickly bring the tracking error to zero.

The SMC strategy has become a popular academic research topic because of its low dependence on the mathematical model of controlled objects and its strong robustness [16]. On the other hand, the switch control law of traditional SMC strategy leads to the chattering phenomenon, the MFiPISMC strategy brings the inherent chattering problem of SMC strategy into the closed loop system. The super-twisting Sliding Mode Control (STSMC) strategy as a high-order SMC scheme, and can effectively eliminate the chattering phenomenon [17]. The STSMC scheme has been widely used in many fields such as the inverted pendulum system [18], unmanned aerial vehicles [19], the photovoltaic system [20], the brushless doubly fed induction generator [21], and so on. A Linear Extended State Observer (LESO) was proposed in References [22,23], which originated from Linear Active Disturbance Rejection Control. The LESO has the advantages of simple structure and efficient estimation, so it has been studied and applied by many scholars [24–27].

Inspired by previous studies and our previous research [28–30], a novel compound model-free control strategy with an intelligent Proportional-Integral and super-twisting Sliding Mode Control (MFiPISTSMC) strategy is proposed. It is worth noting that the proposed MFiPISTSMC strategy is based on the ultra-local model. The MFiPISTSMC strategy solves the problem that the error cannot reach zero quickly in the traditional iPI control strategy of the ultra-local mode, and also deals with the chattering phenomenon of the MFiPISMC strategy. At the same time, the proposed MFiPISTSMC strategy uses the STSMC scheme to improve the control performance of the switching stage. An LESO is integrated into the proposed MFiPISTSMC strategy to estimate the unknown uncertain dynamics of the ultra-local model.

Compared with previous studies, the main contributions of this article can be summarized as follows:

1. A compound MFiPISTSMC strategy is proposed, which integrates the STSMC strategy, the iPI control strategy, and the MFC strategy. The STSMC strategy and the iPI control strategy are all constructed based on the ultra-local model of the PMSM.
2. A novel LESO based on the compound MFiPISTSMC strategy is proposed for the PMSM drives. The stability of the proposed control strategy is proved by the Lyapunov stability theorem. It will be shown from the theoretical discussions that the proposed MFiPISTSMC control strategy can ensure the tracking error of the system tends to zero.
3. The simulation and experimental results show the effectiveness of the proposed model-free hybrid control strategy.

The remaining parts of this paper are arranged as:

In Section 2, the mathematical model of PMSM and the ultra-local model of PMSM are briefly presented. The control strategy and stability analysis are given in in Section 3. The results of simulation and experimental results are shown in Section 4. Finally, concluding observations are contained in Section 5.

2. Problem Formulation

This section presents the mathematical model of PMSM and the ultra-local model of PMSM.

The flux linkage equation, electromagnetic torque equation and voltage equation of salient PMSM are as follows [31]:

$$\begin{cases} \phi_d = L_d i_d + \phi_f \\ \phi_q = L_q i_q \end{cases} \tag{1}$$

$$\begin{cases} u_d = R i_d + \dot{\phi}_d - \omega \phi_q \\ u_q = R i_q + \dot{\phi}_q + \omega \phi_d \end{cases} \tag{2}$$

$$T_e = 1.5 p_n (\phi_f i_q(t) + (L_d - L_q) i_d(t) i_q(t)) \tag{3}$$

When $L_d = L_q = L$ are in this paper, mechanical torque equation is expressed in (4), the dynamic equation of PMSM can be denoted in (5) [31].

$$\begin{cases} T_e - T_L = J\dot{\omega}(t) + B\omega(t) \\ T_e = 1.5 p_n \phi_f i_q(t) \end{cases} \tag{4}$$

$$\dot{\omega}(t) = \frac{3 p_n \phi_f}{2J} i_q(t) - \frac{B}{J}\omega(t) - \frac{1}{J} T_L \tag{5}$$

The key parameters of PMSM are listed in Table 1.

Table 1. Parameters of the permanent magnet synchronous motor (PMSM).

Parameter	Symbol and Unit
Electromagnetic torque	T_e/$N{\cdot}m$
Flux linkage of permanent magnet	ϕ_f/Wb
Pole pairs	p_n/Num
dq-axis inductances	L_d, L_q/mH
dq-stator voltages	u_d, u_q/mH
dq-armature currents	$i_d(t)$, $i_q(t)$/V
dq-axis flux linkages	ϕ_d, ϕ_q/Wb
Mechanical rotor angular speed	$\omega(t)/r{\cdot}s^{-1}$
Rotational inertia	$J/kg{\cdot}m^2$
Load torque	$T_L/N{\cdot}m$
Viscous friction coefficient	$B/N{\cdot}m{\cdot}s$
Stator resistance	R/Ω

According to [11], the general single input single output system can be replaced by the ultra-local model as:

$$y^{(n)}(t) = au(t) + F \tag{6}$$

where $y(t)$ and are the output and input of the ultra-local model, respectively; a is the non-physical constant parameter; F is the unknown term of the system but also any disturbances. In this paper $n = 1$ is satisfied, the first-order system (5) can be selected to describe the dynamics of the controlled system.

The system tracking error is usually defined as:

$$e(t) = y_r(t) - y(t) \tag{7}$$

where $y_r(t)$ is the desired output of the system; $e(t)$ is the system tracking error. The purpose of this paper is to design a stable controller to make the tracking error tend to zero. In this paper, $y(t)$ is the actual value of the mechanical speed; $y_r(t)$ is the given value of the mechanical speed; $e(t)$ is the tracking error of the mechanical speed.

3. Main Results

In this section, the proposed control strategy will be given. Furthermore, the stability of the proposed control strategy will be proved by the Lyapunov stability theorem.

A novel control block diagram of PMSM speed regulation system is based on the proposed MFiPISTSMC strategy and the LESO with d axis current $i_d(t) = 0$ is manifested in Figure 1. The control goal is to make the actual output $y(t)$ tracking the desired output $y_r(t)$. The novel control block diagram of PMSM speed regulation system consists of a proposed MFiPISTSMC strategy, an LESO, a current controller, a voltage source inverter, and a PMSM.

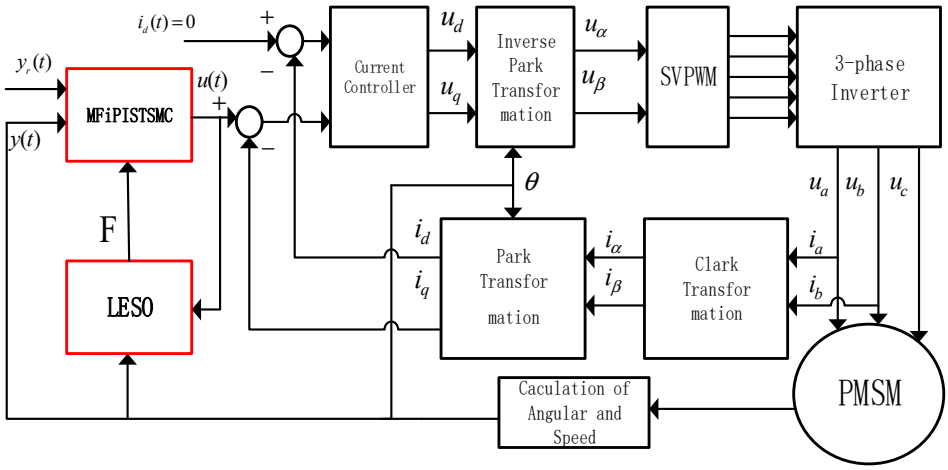

Figure 1. The novel control block diagram using the proposed MFiPISTSMC strategy with $i_d(t) = 0$.

3.1. Design of Unknown Terms Observer

The unknown term of the ultra-local model is estimated by the LESO. For the sake of efficiency and effectiveness, a second order LESO is selected in this paper.

According to (6), define $x_1 = y(t)$ and $x_2 = F$. Equation (6) can be rewritten as:

$$\dot{x}_1 = x_2 + au \tag{8}$$

The second order LESO can be described as [22,23]:

$$\begin{cases} e(t) = Z_{21} - y(t), \\ \dot{Z}_{21} = Z_{22} - \beta_1 e(t) + b_0 u(t), \\ \dot{Z}_{22} = -\beta_2 e(t) \end{cases} \tag{9}$$

where β_1 and β_2 are positive constants; b_0 is the design parameter; Z_{21} and Z_{22} are the estimates of x_1 and x_2, respectively.

3.2. Design of Novel Controller

Theorem 1 [15]. *The iPI control strategy is defined as*:

$$u_1(t) = \frac{1}{a}\left(K_p e(t) + K_i \int e(t)dt + \dot{y}_r(t) - Z_{22}\right) \tag{10}$$

where $K_p > 0$, $K_i > 0$, $u_1(t)$ *is the control law of the iPI control strategy.*

Substituting (10) into (6), the error equation can be obtained:

$$K_p e(t) + K_i \int e(t)dt + \dot{e}(t) + \Delta d(t) = 0 \tag{11}$$

where $\Delta d(t)$ is as follows:

$$\Delta d(t) = F - Z_{22} \tag{12}$$

According to References [15,32], we can get the iPI control strategy that cannot guarantee that the tracking error of the system tends to zero quickly. A detailed description can be found in References [15,32].

The following sliding mode surface is chosen in this paper [33–36]:

$$s(t) = \eta_1 e(t) + \eta_2 \int e(t)dt \tag{13}$$

where η_1 and η_2 are the positive parameters of the sliding mode surface.

Theorem 2. *The proposed MFiPISTSMC strategy is designed in the following format*:

$$\begin{array}{l} u(t) = u_1(t) + u_2(t) \\ = \left\{ \begin{array}{c} \frac{1}{a}\left(K_p e(t) + K_i \int e(t)dt + \dot{y}_r(t) - Z_{22}\right) + u_2(t) \\ u_2(t) = u_{21}(t) + u_{22}(t) \end{array} \right. , \end{array} \tag{14}$$

where $u_2(t)$is the control law of the STSMC strategy; u_{21} is the equivalent control law; u_{22} is the switching control law.

In addition, in order to make the control error of the system rapidly zero, according to (6), (7) and (14), the following equation can be obtained:

$$\dot{e}(t) + au_2 + K_p e(t) + K_i \int e(t)dt + \Delta d(t) = 0 \tag{15}$$

Taking derivative of (13), it can be obtained that:

$$\dot{s}(t) = \eta_1 \dot{e}(t) + \eta_2 e(t) \tag{16}$$

Substituting (15) in (16), the following equation can be obtained:

$$\dot{s}(t) = \eta_1 \left(-au_2 - K_p e(t) - K_i \int e(t)dt - \Delta d(t) \right) + \eta_2 e(t) \tag{17}$$

Ideally, according to (17) and $\Delta d(t) = 0$, the equivalent control law can be obtained as:

$$u_{21} = \frac{1}{a}\left(-K_p e(t) - K_i \int e(t)dt \right) + \frac{\eta_2}{\eta_1 a} e(t) \tag{18}$$

In this paper, the switching control strategy of the MFiPISMC strategy is chosen as:

$$u_{22} = \frac{1}{a}(k_1 sign(s(t)) + k_2 s(t)) \tag{19}$$

where $k_1 \in R^+$, $k_2 \in R^+$.

For compensating external disturbance and eliminating the chattering phenomenon caused by the SMC strategy, the following ST scheme is usually chosen as [17]:

$$\dot{s}(t) = -k_1 \left| s(t) \right|^{1/2} sign(s(t)) - k_2 \int sign(s(t))dt \tag{20}$$

$$sign(s(t)) = \left\{ \begin{array}{cc} 1 & s(t) > 0, \\ 0 & s(t) = 0, \\ -1 & s(t) < 0 \end{array} \right. \tag{21}$$

where k_1 and k_2 are the positive parameters of the ST scheme.

Consequently, the switching control law is obtained as:

$$u_{22} = \frac{1}{a}\left(k_1 |s(t)|^{1/2} sign(s(t)) + k_2 \int sign(s(t))dt\right) \tag{22}$$

Figure 2 describes the structure diagrams of the proposed MFiPISTSMC strategy.

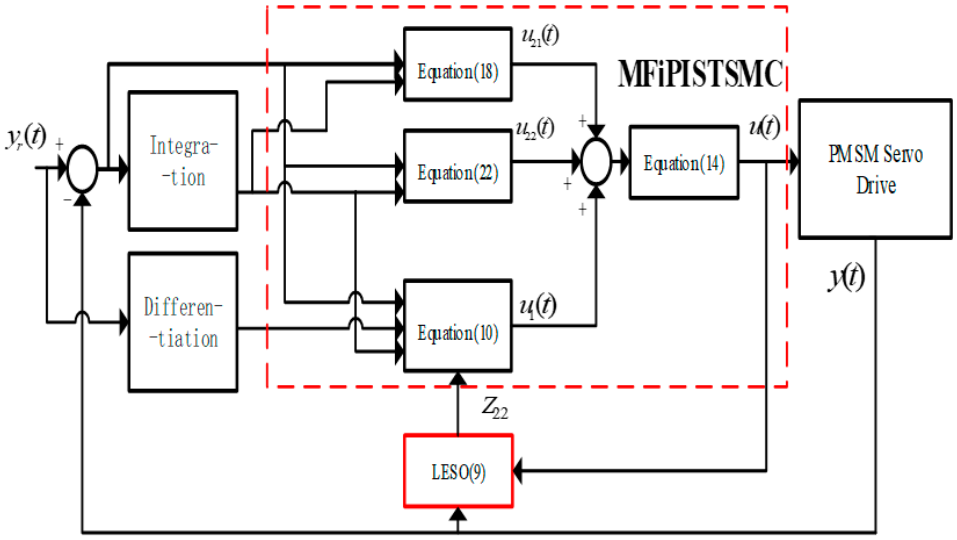

Figure 2. Structure diagram of the proposed MFiPISTSMC strategy.

3.3. Stability Analysis

Inspired by previous studies [17,37–40], the proof of stability is divided into two steps.

Step 1: The stability of the LESO will be discussed. Laplace transform is carried out for (9), and we can get:

$$\begin{cases} Z_{21}(s)s = Z_{22}(s) - 2\lambda Z_{21}(s) + 2\lambda y(s) + b_0 u(s), \\ Z_{22}(s)s = -\lambda^2 Z_{21}(s) + \lambda^2 y(s) \end{cases}$$
$$\begin{cases} Z_{21}(s) = \dfrac{\lambda^2 + 2\lambda s}{(s+\lambda)^2} y(s) + \dfrac{b_0 s}{(s+\lambda)^2} u(s), \\ Z_{22}(s) = \dfrac{\lambda^2 s}{(s+\lambda)^2} y(s) + \dfrac{\lambda^2 b_0}{(s+\lambda)^2} u(s) \end{cases} \tag{23}$$

where λ is the bandwidth of the system.

$$\begin{cases} e_1(s) = Z_{21}(s) - y(s) \\ e_2(s) = Z_{22}(s) - y(s) - b_0 u(s) \end{cases} \tag{24}$$

According to (23), (24) can be rewritten:

$$\begin{cases} e_1(s) = \dfrac{\lambda^2 + 2\lambda s}{(s+\lambda)^2} y(s) + \dfrac{b_0 s}{(s+\lambda)^2} u(s) - y(s), \\ e_2(s) = \dfrac{\lambda^2 s}{(s+\lambda)^2} y(s) + \dfrac{\lambda^2 b_0}{(s+\lambda)^2} u(s) - y(s)s - b_0 u(s) \end{cases}$$
$$\begin{cases} e_1(s) = -\dfrac{s^2}{(s+\lambda)^2} y(s) + \dfrac{b_0 s}{(s+\lambda)^2} u(s), \\ e_2(s) = -\dfrac{s^2 + 2\lambda s}{(s+\lambda)^2} y(s)s - \dfrac{s^2 + 2\lambda s}{(s+\lambda)^2} b_0 u(s) \end{cases} \tag{25}$$

According to [37], when $s \to 0$, we can get $se_1(s) \to 0$ and $se_2(s) \to 0$, therefore, the LESO exhibits stability.

Step 2: In what follows, the stability of the proposed MFiPISTSMC strategy will be discussed.

Assumption 1. *The value of* $\left|\Delta\dot{d}(t)\right|$ *has an upper limit, and the estimation error of the LESO satisfies the following condition*:

$$\left|\Delta\dot{d}(t)\right| \le \Psi, \tag{26}$$

where Ψ *is a positive constant. The condition (26) shows the estimation error of the LESO is a bounded perturbation.*

In order to guarantee the stability of the proposed MFiPISTSMC strategy, we do the following steps: By substituting (14) into (17), we obtain the following:

$$\begin{aligned} \dot{s}(t) &= \eta_1\left(-au_2 - K_p e(t) - K_i\int e(t)dt - \Delta d(t)\right) + \eta_2 e(t) \\ &= -k_1\eta_1\left|s(t)\right|^{1/2} sign(s(t)) - k_2\eta_1\int sign(s(t))dt - \eta_1\Delta d(t) \end{aligned} \tag{27}$$

Equation (27) can be shown as:

$$\begin{cases} \dot{s}(t) = -k_1\eta_1\left|s(t)\right|^{1/2} sign(s(t)) - \eta_1\Delta d(t) + \Phi \\ \dot{\Phi} = -k_2\eta_1 sign(s(t)) \end{cases} \tag{28}$$

Defining the following new variables as:

$$\begin{cases} x_1 = s(t) \\ x_2 = -\eta_1\Delta d(t) + \Phi \end{cases} \qquad \begin{cases} \dot{x}_1 = -k_1\eta_1|x_1|^{1/2} sign(x_1) + x_2 \\ \dot{x}_2 = -k_2\eta_1 sign(x_1) - \eta_1\Delta\dot{d}(t) \end{cases} \tag{29}$$

The following Lyapunov function is chosen:

$$\begin{cases} V = \zeta^T P\zeta \\ \zeta^T = \begin{bmatrix} |x_1|^{1/2} sign(x_1) & x_2 \end{bmatrix} \end{cases} \tag{30}$$

where P is a positive definite matrix which can be selected in accordance with the procedure given in [39]; V is a quadratic, strict, and robust Lyapunov function.

Actually, according to Assumption 1, we can get:

$$\dot{V} \le -|x_1|^{1/2}\zeta^T X\zeta \tag{31}$$

where X is a symmetric and positive definite matrix. We can get $\dot{V}$ is negative semi-definite. A detailed description can be found in the Reference [39].

Accordingly, the proposed controller can ensure the stability of the system. Consequently, the proof of the closed-loop system under the proposed MFiPISTSMC strategy is completed.

4. Simulation and Experimental Results

4.1. Simulink Results

We implement the simulation, which are based on the Matlab/Simulink. The key PMSM parameters used in the simulation are listed as follows: the stator phase resistance R is 2.875 Ω; the inductance L is 8.5 mH; the magnetic chain of permanent magnets ϕ is 0.175 Wb; the moment of inertia J is 0.003 $kg{\cdot}m^2$;

the viscous damping B is 0.008 $N{\cdot}m{\cdot}s$; the pole pairs p_n is 4. The parameters of the MFiPISMC strategy used in the simulation are listed as follows: $K_p = 1$; $K_i = 1$; $\eta_1 = 10$; $\eta_2 = 1$; $k_1 = 10$; $k_2 = 12$; $a = 1000$. The parameters of the PI strategy used in the simulation are listed as follows: the value of proportional coefficient set to 0.1; the value of integral coefficient set to 0.5. The parameters of the proposed MFiPISTSMC strategy used in the simulation are listed as follows: $K_p = 1$; $K_i = 1$; $\eta_1 = 10$; $\eta_2 = 1$; $k_1 = 300$; $k_2 = 100$; $a = 1000$. The parameters of the LESO used in the simulation are listed as follows: $\beta_1 = 20000$; $\beta_2 = 1500000$; $b_0 = 1000$. In order to compare more accurately, the stable simulation data from 0.2 to 0.5 s are used to perform the following calculations:

$$\text{Rootmean Square Error (RMSE)} = \sqrt{\sum_1^N e(t)_i^2 / N} \tag{32}$$

$$\text{Maximum Absolute Error (MAE)} = Max\left|e_i(t)\right| \tag{33}$$

The PI control strategy and the MFiPISMC strategy are compared with the control strategy proposed in this study. In order to compare the control performance of various controllers, the reference speed is set to 100 r/s and the simulation time is set to 0.5 s. Figure 3 and Table 2 compare the speed response curves of the motor under different control strategies without load starting and stable operation. Moreover, Figure 4 and Table 3 compare the speed response curves of the motor under different control strategies with 0.5 $N{\cdot}m$ load starting and stable operation. As shown in Figure 3a or Figure 4a, compared with the PI control strategy and MFiPISMC strategy, the adjustment time controlled by the proposed MFiPISTSMC strategy is the shortest, which indicates that the proposed MFiPISTSMC strategy has the optimal transient performance. As shown in Tables 2 and 3, compared with the PI control strategy and MFiPISMC strategy, the RMSE and MAE controlled by the proposed MFiPISTSMC strategy also are the smallest, which reveal that the proposed MFiPISTSMC strategy has the optimal control accuracy. From Figure 3b or Figure 4b, we also can obviously conclude that the chattering phenomenon of the proposed MFiPISTSMC strategy has been eliminated significantly. Consequently, the proposed MFiPISTSMC strategy has the best steady-state performance.

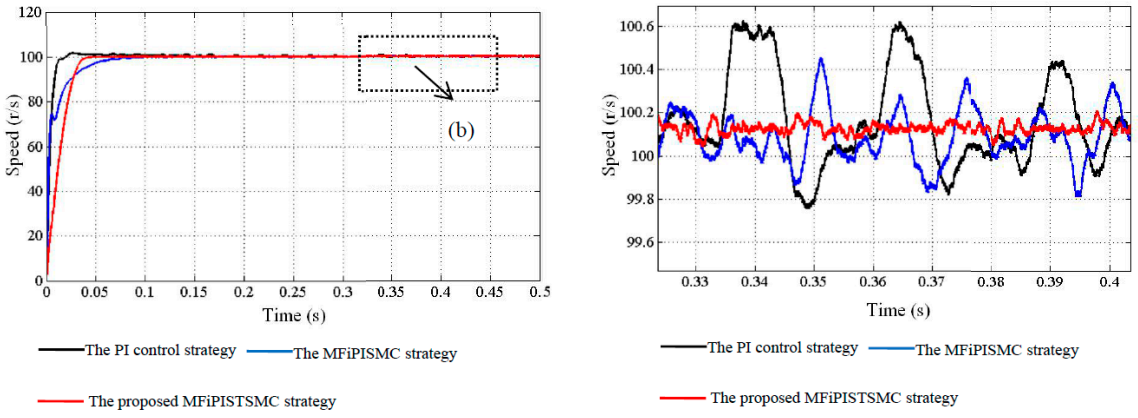

Figure 3. (**a**) Speed response curves with $\omega_r = 100\ r/s$ without load starting and stable operation; (**b**) detailed view of the image (**a**).

Table 2. The comparative results of the speed response curves without load.

Control Strategy	Desired Speed (r/s)	Settling Time (s)	RMSE (r/s)	MAE (r/s)
The PI control strategy	100	0.082	0.303	0.632
The MFiPISMC strategy	100	0.071	0.155	0.485
The proposed MFiPISTSMC strategy	100	0.049	0.131	0.243

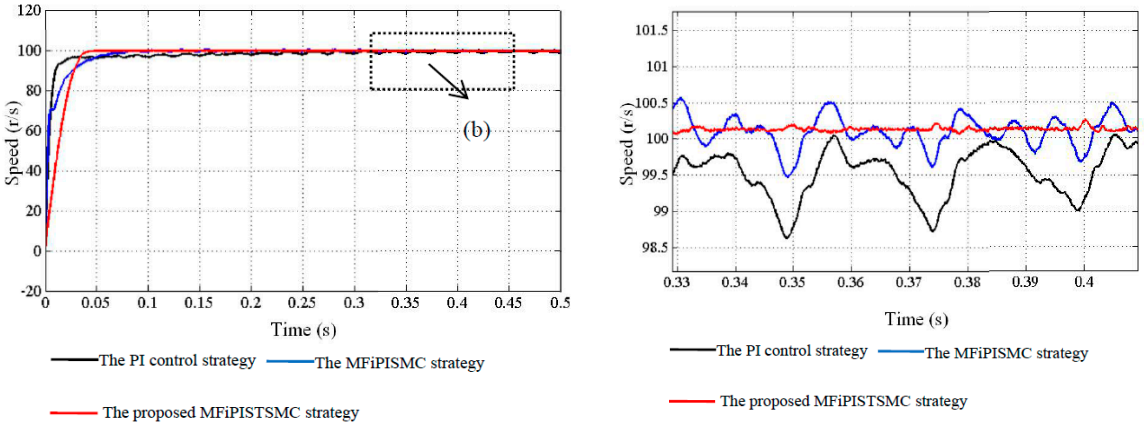

Figure 4. (**a**) Speed response curves with $\omega_r = 100\ r/s$ with 0.5 $N{\cdot}m$ load starting and stable operation; (**b**) detailed view of the image (**a**).

Table 3. The comparative results of the speed response curves with load.

Control Strategy	Desired Speed (r/s)	Settling Time (s)	RMSE (r/s)	MAE (r/s)
The PI control strategy	100	0.182	0.767	1.547
The MFiPISMC strategy	100	0.075	0.234	0.618
The proposed MFiPISTSMC strategy	100	0.043	0.137	0.312

In order to further verify the anti-disturbance ability of the proposed control strategy, load disturbances are suddenly changed at 0.5 and 1 s, respectively. Tables 4 and 5 show the comparative results of load changed suddenly under different control strategies, including speed perturbation, speed recovery time, and torque adjustment time. Figures 5 and 6 compare the speed response curves and the torque response curves under different control strategies with the load changed suddenly. As shown in Tables 4 and 5 and Figures 5 and 6, compared with the PI control strategy and MFiPISMC strategy, the speed recovery time and torque adjustment time controlled by the proposed MFiPISTSMC strategy are the shortest, the speed perturbation amplitude controlled by the proposed MFiPISTSMC strategy is also the smallest, which indicates that the proposed MFiPISTSMC strategy has stronger robustness and better reliability when subjected to external uncertainties.

Table 4. The comparative results of the load increased suddenly.

Control Strategy	**The External Load Becomes** 0.5 $N{\cdot}m$ **from** 0 $N{\cdot}m$		
	Speed Perturbation Amplitude (%)	**Speed Recovery Time (s)**	**Torque Adjustment Time (s)**
The PI control strategy	5.3	0.456	0.012
The MFiPISMC strategy	2.5	0.052	0.005
The proposed MFiPISTSMC strategy	0.4	0.018	0.002

Table 5. The comparative results of the load decreased suddenly.

Control Strategy	**The External Load Becomes** 0 **from** 0.5 $N{\cdot}m$		
	Speed Perturbation Amplitude (%)	**Speed Recovery Time (s)**	**Torque Adjustment Time (s)**
The PI control strategy	5.6	0.462	0.011
The MFiPISMC strategy	2.9	0.049	0.006
The proposed MFiPISTSMC strategy	0.7	0.012	0.003

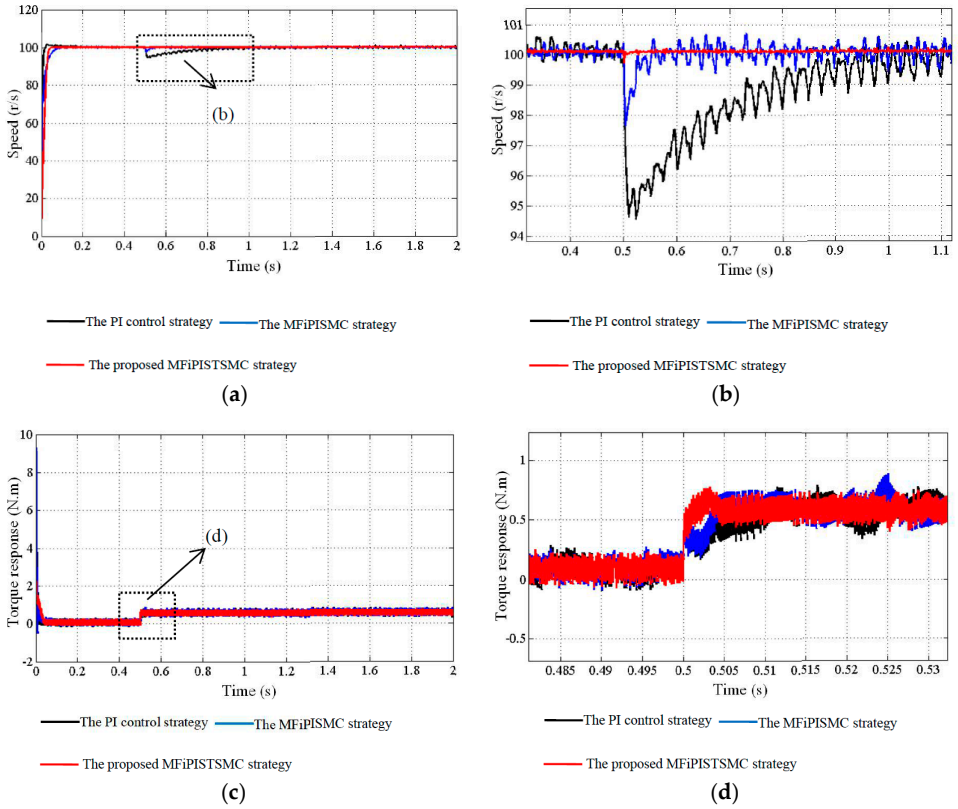

Figure 5. (**a**) Speed response curves with load increased suddenly; (**b**) detailed view of the image (**a**); (**c**) torque response curves in the case of load suddenly increases; (**d**) detailed view of the image (**c**).

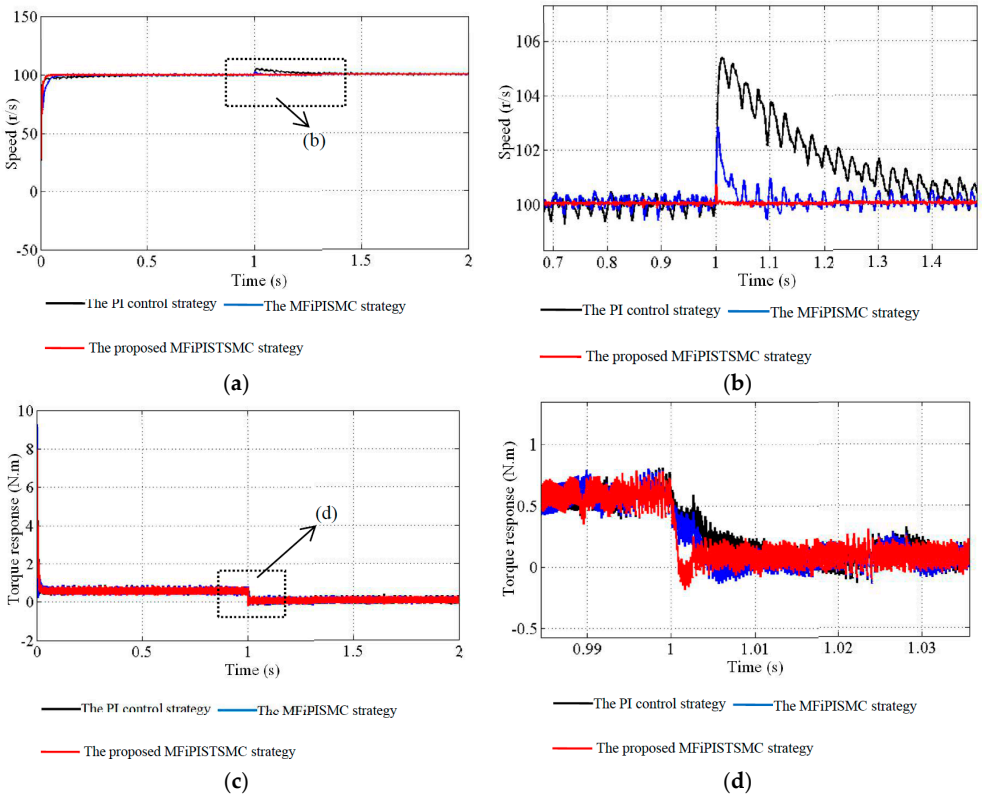

Figure 6. (**a**) Speed response curves with load decreased suddenly; (**b**) detailed view of the image (**a**); (**c**) torque response curves in the case of load suddenly decreases; (**d**) detailed view of the image (**c**).

4.2. Experimental Results

To further verify the effectiveness of the proposed method, a cSPACE (Control signal process and control engineering) based PMSM speed control experimental platform has been applied in this paper. The cSPACE experimental platform of the PMSM drive system is depicted in Figure 7. The cSPACE experimental platform consists of a TI TMS320F28335 DSP, a Matlab/Simulink, a SM060R20B30M0AD PMSM, and a MY1016 DC generator. The cSPACE experimental platform is the software and hardware platform of fast control prototype and hardware in loop real-time simulation.

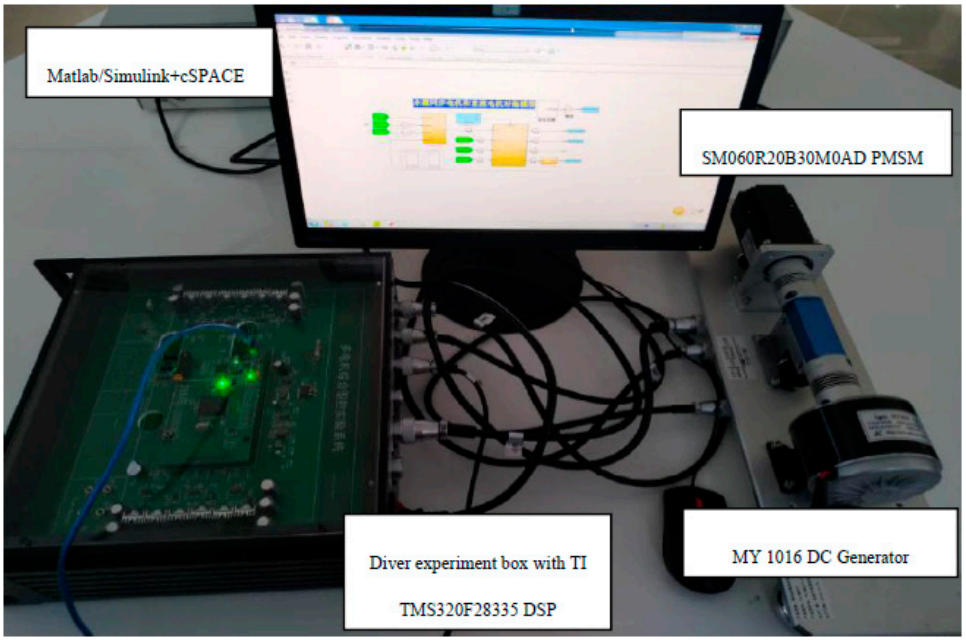

Figure 7. The PMSM experimental platform.

The key PMSM parameters used in the experimentation are listed as follows: the stator phase resistance R is 0.16 Ω; the inductance L is 0.44 mH; the magnetic chain of permanent magnets ϕ is 0.0077 Wb; the moment of inertia J is 0.342 $kg{\cdot}m^2{\cdot}10^{-4}$; the viscous damping B approximately is zero; the pole pairs p_n is 4. The parameters of the proposed MFiPISTSMC strategy used in the experimentation are listed as follows: $K_p = 1$; $K_i = 0.01$; $\eta_1 = 1$; $\eta_2 = 1$; $k_1 = 500$; $k_2 = 10$; $a = 1000$. The parameters of the LESO used in the experimentation are listed as follows:$\beta_1 = 20000$; $\beta_2 = 1500000$; $b_0 = 1000$. Besides, the saturation limit of $u(t)$ is set to $\pm 10A$.

Figure 8 shows the actual speed response curves of tracking 100 r/s and 300 r/s under the PI control strategy based on the cSPACE experimental platform. Figure 9 shows the actual speed response curves of tracking 100 r/s and 300 r/s under the proposed MFiPISTSMC strategy based on the cSPACE experimental platform. Figure 10 and Table 6 show the comparative results of the dynamic experiments. Because the control strategy is written as discrete form on the experimental platform, the horizontal coordinates of the experimental results are the sampling points. From the experimental results presented in Table 6 and Figures 8–10, we can clearly find that the actual speed response curves of the PMSM using the proposed MFiPISTSMC strategy can track the set speed value more quickly. The experimental results also reveal that the proposed MFiPISTSMC strategy has the optimal control accuracy. It is a fact that the proposed MFiPISTSMC strategy has the superior dynamic and static characteristics.

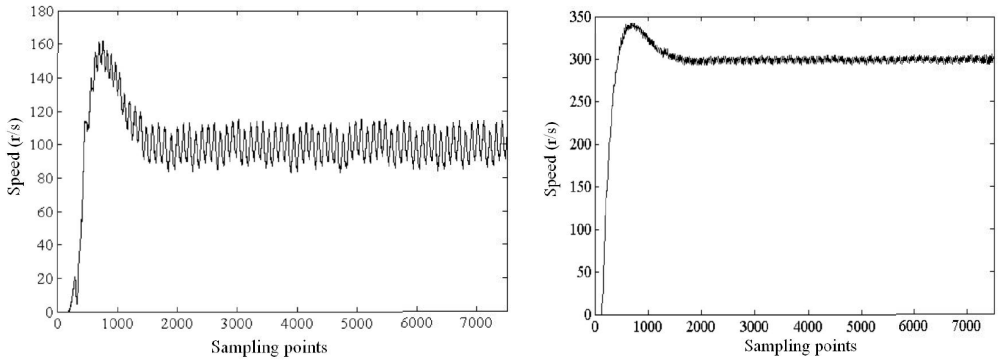

(**a**) (**b**)

Figure 8. (**a**) The experimental speed response curves starting and stable operation with $\omega_r = 100\ r/s$ using the PI control strategy; (**b**) the experimental speed response curves starting and stable operation with $\omega_r = 300\ r/s$ using the PI control strategy.

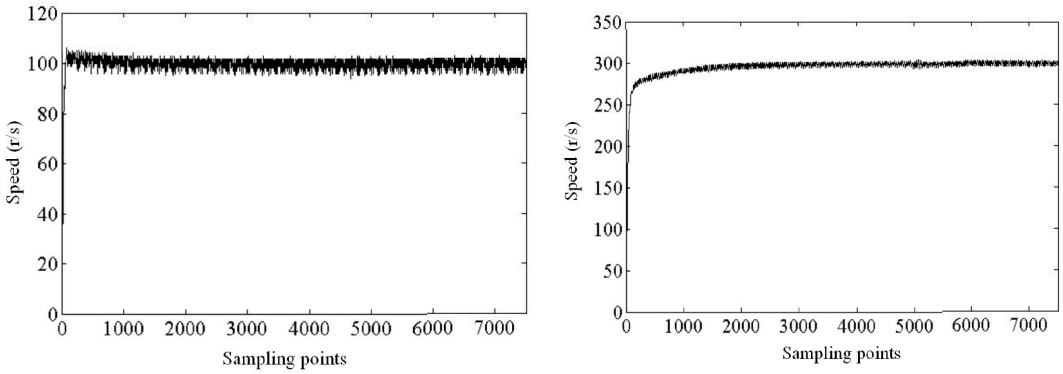

(**a**) (**b**)

Figure 9. (**a**) The experimental speed response curves starting and stable operation with $\omega_r = 100\ r/s$ using the proposed MFiPISTSMC strategy; (**b**) the experimental speed response curves starting and stable operation with $\omega_r = 300\ r/s$ using the proposed MFiPISTSMC strategy.

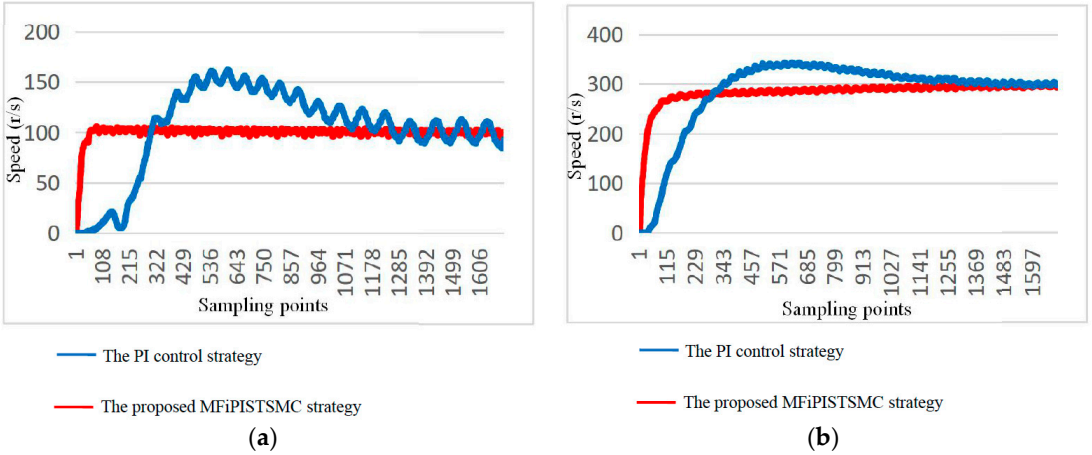

(**a**) (**b**)

Figure 10. (**a**) The comparison of dynamic experiments with $\omega_r = 100\ r/s$ (**b**) the comparison of dynamic experiments with $\omega_r = 300\ r/s$.

When the PMSM is subjected to the external disturbance, the abilities of the PI control strategy and the proposed MFiPISTSMC strategy to resist the external disturbance are shown in Figures 11 and 12, respectively. In detailing, we sample 16,000 points in the experiment. The external load current of the MY1016 DC generator suddenly becomes 200 mA from 0 mA at sampling point 7000 in Figures 11 and 12,

respectively. The external load current of the MY1016 DC generator suddenly becomes 0 mA from 200 mA at sampling point 13,000 in Figures 11 and 12, respectively. From the experimental results, it can be concluded that the proposed MFiPISTSMC strategy has strong anti-disturbance ability and better reliability for suddenly increases and suddenly decreases of load disturbance. It can be clearly observed that the proposed MFiPISTSMC strategy can conveniently suppress the external disturbances.

Table 6. The comparative results of the dynamic experiments.

Control Strategy	The Results of the Dynamic Experiments with ω_r = 100 *r/s*		The Results of the Dynamic Experiments with ω_r = 300 *r/s*	
	Overshoot (%)	Adjustment Time (Sampling Point)	Overshoot (%)	Adjustment Time (Sampling Point)
The PI control strategy	54.2	1203	14.2	1150
The proposed MFiPISTSMC strategy	4.5	157	2.3	491

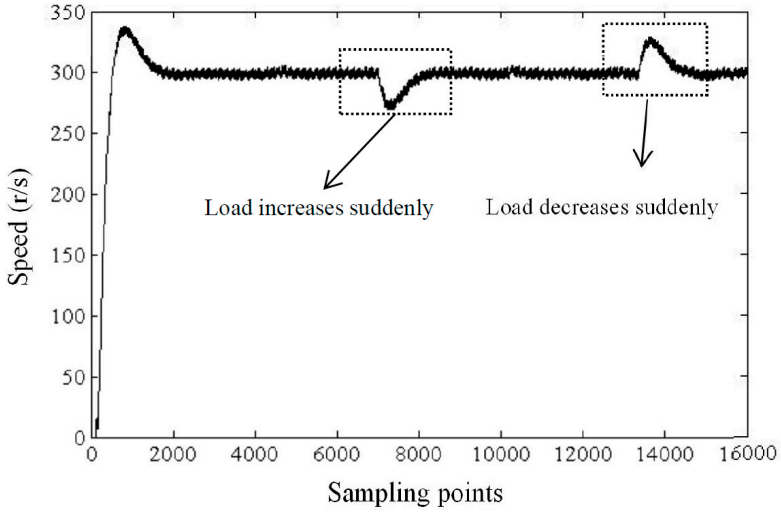

Figure 11. The experimental speed response with load changed suddenly using the Proportional-Integral (PI) control strategy.

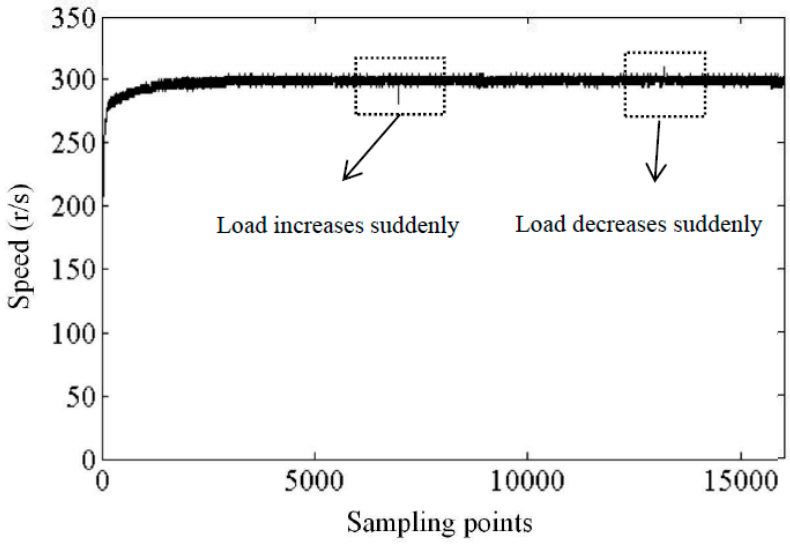

Figure 12. The experimental speed response with load changed suddenly using the proposed MFiPISTSMC strategy.

In summary, the experimental results demonstrate the proposed MFiPISTSMC strategy achieves superior control performance in the sense of the dynamic characteristic, static characteristic, robustness, and reliability.

5. Conclusions

In this research, a novel compound MFiPISTSMC strategy based on the ultra-local model is proposed for the control of the PMSM speed regulation system. The unknown term of the ultra-local model of PMSM is estimated by the LESO. The Lyapunov approach is used to demonstrate the stability of the closed-loop system. The proposed compound MFiPISTSMC strategy consists of the STSMC strategy, the iPI control strategy, and the MFC strategy, which has excellent performance. The static characteristic, dynamic characteristic, robustness, and reliability of the novel compound MFiPISTSMC strategy are verified by simulation and experimental results.

In the future, we will introduce the Fractional-order theory into the compound MFiPISTSMC strategy, which can further improve the control effect.

Author Contributions: This is a joint work and the authors were in charge of their expertise and capability: P.G. for investigation, analysis and writing; G.Z. for funding support. X.L. for manuscript revision. All authors have read and agreed to the published version of the manuscript.

Funding: This research was supported by the National Natural Science Foundation of China under Grant (no.61703202) and by the Key Research Development Project of Jiangsu Province under Grant BE (no.2017164).

Acknowledgments: The authors would like to express their gratitude to all those who helped them during the writing of this paper. Furthermore, the authors would like to thank the reviewers for their valuable comments and suggestions.

Conflicts of Interest: The authors declare no conflict of interest.

References

1. Tsampouris, E.M.; Beniakar, M.E.; Kladas, M.E. Geometry optimization of PMSMs comparing full and fractional pitch winding configurations for aerospace actuation applications. *IEEE Trans. Manag.* **2012**, *48*, 943–946. [CrossRef]
2. Li, H.; Chen, T.; Yao, H. Mechanism, diagnosis and development of demagnetization fault for pmsm in electric vehicle. *Trans. China Electrotech. Soc.* **2013**, *8*, 276–284.
3. Talla, J.; Leu, V.Q.; Smidl, V.; Peroutka, Z. Adaptive RBF network based direct voltage control for interior PMSM based vehicles. *IEEE Trans. Ind. Electron.* **2018**, *65*, 8532–8542. [CrossRef]
4. Kang, B.J.; Liaw, C.M. A robust hysteresis current-controlled PWM inverter for linear PMSM driven magnetic suspended positioning system. *IEEE Trans. Ind. Electron.* **2001**, *48*, 956–967. [CrossRef]
5. Luo, Y.; Liu, C. A simplified model predictive control for a dual three-phase PMSM motor with reduced harmonic currents. *IEEE Trans. Ind. Electron.* **2018**, *65*, 9079–9089. [CrossRef]
6. Kim, S.K.; Lee, J.S.; Lee, K.B. Offset-free robust adaptive back-stepping speed control for uncertain permanent magnet synchronous motor. *IEEE Trans. Power Electron.* **2016**, *31*, 7065–7076. [CrossRef]
7. Chen, J.; Yao, W.; Ren, Y.; Wang, R.; Zhang, L.; Jiang, L. Nonlinear adaptive speed control of a permanent magnet synchronous motor: A perturbation estimation approach. *Automatica* **2017**, *76*, 143–152. [CrossRef]
8. Wang, W.; Shen, H.S.; Hou, L.M.; Gu, H.W.H. Robust control of permanent magnet synchronous motor based on PCHD. *J. Autom. Sin.* **2015**, *2*, 143–150. [CrossRef]
9. Liu, T.T.; Tan, Y.; Wu, G.; Wang, S.M. Simulation of PMSM Vector Control System Based on Matlab/Simulink. In Proceedings of the IEEE International Conference on Measuring Technology and Mechatronics Automation (ICMTMA' 2009), Zhangjiajie, Hunan, China, 11–12 April 2009; pp. 343–346.
10. Qian, J.; Ji, C.; Pan, N.; Wu, J. Improved sliding mode control for permanent magnet synchronous motor speed regulation system. *Appl. Sci.* **2018**, *8*, 2491. [CrossRef]
11. Fliess, M.; Join, C. Intelligent PID Controllers. In Proceedings of the 16th Mediterranean Conference on Control and Automation Congress Centre, Ajaccio, France, 25–27 June 2008.
12. Agee, J.T.; Kizir, S.; Bingul, Z. Intelligent proportional-integral (iPI) control of a single link flexible joint manipulator. *J. Sound Vibrat.* **2015**, *21*, 2273–2288. [CrossRef]

13. Al Younes, Y.; Drak, A.; Noura, H.; Rabhi, A. Model-free control of a quadrotor vehicle. In Proceedings of the 2014 International Conference on Unmanned Aircraft Systems, ICUAS'14, Orlando, FL, USA, 27–30 May 2014; pp. 1126–1131.
14. Doye, I.N.; Asiri, S.; Aloufi, A.; Al-Awan, A.; Laleg-Kirati, T.-M. Intelligent proportional integral derivative control-based modulating functions for laser beam pointing and stabilization. *IEEE Trans. Control Syst. Technol.* **2020**, *28*, 1001–1008. [CrossRef]
15. Li, S.; Wang, H.; Tian, Y.; Aitouch, A.; Klein, J. Direct power control of DFIG wind turbine systems based on an intelligent proportional-integral sliding mode control. *ISA Trans.* **2016**, *64*, 431–439. [CrossRef]
16. Wang, Y.; Feng, Y.; Zhang, X.; Liang, J. A new reaching law for antidisturbance sliding-mode control of PMSM speed regulation system. *IEEE Trans. Power Electron.* **2020**, *35*, 4117–4126. [CrossRef]
17. Levant, A. Robust exact differentiation via sliding mode technique. *Automatica* **1998**, *34*, 379–384. [CrossRef]
18. Chalanga, A.; Patil, M.; Bandyopadhyay, B.; Arya, H. Output regulation using new sliding surface with an implementation on inverted pendulum system. *Eur. J. Control* **2019**, *45*, 85–91. [CrossRef]
19. Ha, L.N.N.T.; Hong, S.K. Robust Dynamic Sliding Mode Control-Based PID–Super Twisting Algorithm and Disturbance Observer for Second-Order Nonlinear Systems: Application to UAVs. *Electronics* **2019**, *8*, 760. [CrossRef]
20. Zebbar, M.; Messlem, Y.; Gouichiche, A.; Tadjine, M. Super-twisting sliding mode control and robust loop shaping design of RO desalination process powered by PV generator. *Desalination* **2019**, *458*, 122–135. [CrossRef]
21. Sadeghi, R.; Madani, S.M.; Ataei, M.; Agha Kashkooli, M.R.; Ademi, S. Super-twisting sliding mode direct power control of brushless doubly fed induction generator. *IEEE Trans. Ind. Electron.* **2018**, *65*, 9147–9156. [CrossRef]
22. Gao, Z. Active Disturbance Rejection Control: A Paradigm Shift in Feedback Control System Design. In Proceedings of the 2006 American Control Conference, Minneapolis, MA, USA, 14–16 June 2006; pp. 2399–2405.
23. Gao, Z.; Huang, Y.; Han, J. An Alternative Paradigm for Control System Design. In Proceedings of the 40th IEEE Conference on Decision and Control, Orlando, FL, USA, 4–7 December 2001.
24. Zhang, B.; Tan, W.; Li, J. Tuning of linear active disturbance rejection controller with robustness specification. *ISA Trans.* **2019**, *85*, 237–246. [CrossRef]
25. Wang, G.; Liu, R.; Zhao, N.; Ding, D.; Xu, D. Enhanced linear ADRC strategy for HF pulse voltage signal injection-based sensorless IPMSM drives. *IEEE Trans. Power Electron.* **2018**, *34*, 514–525. [CrossRef]
26. Wang, Y.W.; Zhang, W.A.; Yu, L. A linear active disturbance rejection control approach to position synchronization control for networked interconnected motion system. *IEEE Trans. Control Netw. Syst.* **2020**, *8*, 1. [CrossRef]
27. Zhou, X.; Wang, C.; Ma, Y. Vector speed regulation of an asynchronous motor based on improved first-order linear active disturbance rejection technology. *Energy* **2020**, *13*, 2168.
28. Gao, P.; Zhang, G.M.; Ouyang, H.M.; Mei, L. A sliding mode control with nonlinear fractional order PID sliding surface for the speed operation of surface-mounted PMSM drives based on an extended state observer. *Math. Probl. Eng.* **2019**, *2019*, 7130232. [CrossRef]
29. Gao, P.; Zhang, G.M.; Lv, X.D. A novel compound nonlinear state error feedback super-twisting fractional-order sliding mode control of PMSM speed regulation system based on extended state observer. *Math. Probl. Eng.* **2020**, *2020*, 1843598. [CrossRef]
30. Gao, P.; Zhang, G.M.; Ouyang, H.M.; Mei, L. An adaptive super twisting nonlinear fractional order PID sliding mode control of permanent magnet synchronous motor speed regulation system based on extended state observer. *IEEE Access* **2020**, *8*, 53498–53510. [CrossRef]
31. Sira-Ramirez, H.; Linares-Flores, J.; Garcia-Rodriguez, C.; Contreras-Ordaz, M.A. On the control of the permanent magnet synchronous motor: An active disturbance rejection control approach. *IEEE Trans. Control. Syst. Technol.* **2014**, *22*, 2056–2063. [CrossRef]
32. Wang, H.P.; Mustafa, G.I.; Tian, Y. Model-free fractional-order sliding mode control for an active vehicle suspension system. *Adv. Eng. Softw.* **2018**, *115*, 452–461. [CrossRef]
33. Li, S.; Zhou, M.; Yu, X. Design and implementation of terminal sliding mode control method for PMSM speed regulation system. *IEEE Trans. Ind. Inf.* **2013**, *9*, 1879–1891. [CrossRef]

34. Zhao, L.; Dai, L.W.; Xia, Y.Q.; Li, P. Attitude control for quadrotors subjected to wind disturbances via active disturbance rejection control and integral sliding mode control. *Mech. Syst. Signal. Pract.* **2019**, *129*, 531–545. [CrossRef]
35. Zhang, X.; Sun, L.; Zhao, K.; Sun, L. Nonlinear speed control for PMSM system using sliding mode control and disturbance compensation techniques. *IEEE Trans. Power Electron.* **2013**, *28*, 1358–1365. [CrossRef]
36. Qu, L.Z.; Qiao, W.; Qu, L.Y. An extended-state-observer-based sliding-mode speed control for permanent-magnet synchronous motors. *IEEE J. Emerg. Select. Top. Power Electron.* **2020**, *99*, 1. [CrossRef]
37. Liu, B.Y.; Zhu, C.A.; Guo, X.Z. Current-loop control for the pitching axis of aerial cameras via an improved ADRC. *Math. Probl. Eng.* **2017**, *6*, 1–8. [CrossRef]
38. Merabet, A. Cascade second order sliding mode control for permanent magnet synchronous motor drive. *Electronics* **2019**, *8*, 1508. [CrossRef]
39. Moreno, J.A.; Osorio, M. Strict Lyapunov functions for the super-twisting algorithm. *IEEE Trans. Automat. Control* **2012**, *57*, 1035–1040. [CrossRef]
40. Goel, A.; Mobayen, S.; Fekih, A. A homogeneous extended state estimator-based super-twisting sliding mode compensator for matched and unmatched uncertainties. *Meas. Control* **2020**, *8*, 002029402092227. [CrossRef]